THE CUMULANT ANALYSIS OF THE DISTRIBUTION OF IMPLANTED IONS

V.V. ILYINA, M.V. MAKARETS'

Taras Shevchenko Kyiv National University
(6, Academician Glushkov Prosp., Kyiv 03127, Ukraine; e-mail: mmv@mail.univ.kiev.ua)

UDC 539

The method of analysis of the Lindhard—Scharff—Schiott (LSS) equations which was proposed earlier by the authors for the distribution of total ion paths is applied to the spatial distribution of implanted ions. The integral equations for eight first cumulants are obtained, and their solutions are calculated for one-component targets for ion energies from 100 eV to 1 GeV. The general features of the energy dependences of distribution parameters are found, and it is shown that a fitting of the distribution to experimental results can give essential correlated errors in the obtained parameters. The method allows one to take into account all the distribution moments in the determination of the form of atom-atom interaction.

Introduction

The most important macroscopic characteristics of ion implantation are the spatial distributions of implanted ions and energy losses caused by various interaction mechanisms of ions with a target. This has stimulated the development of different methods for their measurements and calculations. Their short description, advantages, and drawbacks are illustrated in [1]. The so-called cumulant algorithm was also proposed to analyze the distribution of total ion ranges. This algorithm has the following advantages: 1) contributions of a nuclear scattering and an electronic stopping to cumulants are shown explicitly; 2) it allows one to determine the atom-atom interaction more precisely by using higher cumulants of the ion distribution; 3) a very fast and exact algorithm can be created for the calculations of cumulants of the distribution of total ion ranges in infinite one-component targets for ion energies from 100 eV up to 1 GeV; 4) an exact formal expression for the total range distribution function can be found.

The recent *ab-initio* calculations [2] have shown that the ion-fullerene interaction has the nuclear scattering and electronic stopping that are essentially different from those predicted by the LSS-theory [3]. On the other hand, it is well known [4] that errors of Monte Carlo calculations can attain 100% and even more for only the second moments of the distribution of implanted ions. These errors are caused by an inaccuracy in the description of the nuclear and electron interactions. Being assumed to be additive and independent quantities, they are chosen to fulfil the condition of equality of the calculated and experimental ranges of ions. However, the high-order calculated moments can be rather different from the experimental ones. Apparently, the error can be reduced if the experimental data for high-order moments are taken into account to describe the atom-atom interaction more precisely. On the other hand, it can also be achieved by more accurate calculations of the atom-atom interaction in solids, where a theoretical basis would be wider than the Thomas—Fermi atom model. The second manifestation of this physical problem is the influence of a solid surface on the distribution. As an isotropic, homogeneous, and infinite solid is assumed in theory, the atom-atom interaction is constant inside it.

Moreover, the LSS-theory has other problems which are connected with its basic assumptions which are not physical. There is no regular and reliable method for the reconstruction of a distribution function by using higher-order moments as it is a pure mathematical

problem [5]. Only simplified approximations are used which have two, three, and four parameters [1, 3, 6–8] in opposite to the real distribution which has the infinite number of parameters. This creates the problem of interpretation of experimental data, because they are usually found by fitting theoretical curves with unknown parameters to experimental ones. However, if a theoretical curve is wrong, the corresponding results of the fitting are wrong too. There are also some numerical and computational difficulties resulted from the fact that the equations for spatial moments are very cumbersome, and the corresponding numerical algorithms usually lose stability for the energy of ions higher than about 10 MeV. These reasons are a hindrance for the accurate and full comparison of experimental data on the distributions of implanted ions with theoretical predictions.

The purpose of this paper is: 1) to apply the cumulant algorithm to solving the LSS-equations for parameters of the spatial distribution of ions; 2) to test its numerical accuracy and to compare it with other methods; 3) to test a possibility of the usage of higher moments of the distribution to determine details of the nuclear and electronic interactions.

1. Cumulants and the Spatial Distribution of Ions

Let $\Pi(r,\theta,E)dV$ be the probability of that an ion starting with energy E from the origin of coordinates along the x-axis will stop in an infinitesimal volume dV with the coordinates $x = r\cos\theta$, $y = r\sin\theta\sin\phi$, $z = r\sin\theta\cos\phi$.

On the one hand, we can describe and analyze it by using moments of the distribution $\langle x^l y^m z^n\rangle \equiv T_{lmn} = T_{lnm}$ of the order $N = l+m+n$ which are expressed as

$$T_{lmn} = \int_0^{\infty}\int_0^{\pi}\int_0^{2\pi} r^{l+m+n+2}\Pi(r,\theta,E)\cos^l \times$$

$$\times\theta\sin^{m+n+1}\theta\sin^m\phi\cos^n\phi dr d\theta d\phi, \qquad (1)$$

and then we can obtain usual equations for these or similar moments [3, 6].

On the other hand, we can use the second characteristic function of a general spatial distribution of ions $\Pi(x,y,z,E)$ which is a natural logarithm of its Fourier transformation [9] expressed as

$$\Phi(u,v,w,E) = \sum_{l,m,n=1}^{\infty} i^{l+m+n}\frac{u^l v^m w^n}{l!m!n!}\kappa_{lmn}(E), \qquad (2)$$

where u, v, w are coordinates of the inverse space, $\kappa_{lmn}(E)$ are cumulants of the distribution with the same order as above. They are connected with the moments T_{ijk} [5, 9]. If we take into account the symmetry of $\Pi(r,\theta,E)$ and denote $\kappa_{lmn} \Rightarrow \chi_{lk}$, where $k = m+n$, then we obtain

$$\Phi = -\frac{1}{2}\Big[u^2\chi_{20} + (v^2+w2)\chi_{02} - \frac{2}{4!}(u^4\chi_{40} +$$

$$+6u^2(v^2+w^2)\chi_{22} + (v^2+w^2)^2\chi_{04})\Big] +$$

$$+iu\Big[\chi_{10} - \frac{1}{3!}(u^2\chi_{30} + 3(v^2+w^2)\chi_{12})\Big]\ldots \qquad (3)$$

The following relations are valid [1, 5, 9] for cumulants and usual distribution parameters:

$$R_p = \chi_{10}; \quad \triangle R_p = \sqrt{\chi_{20}}, \quad \triangle Y = \sqrt{\chi_{02}};$$

$$\mathrm{Sk} = \chi_{30}/\chi_{20}^{3/2}, \quad \beta_{12} = \chi_{12}/(\sqrt{\chi_{20}}\chi_{02});$$

$$\mathrm{Ex}_{\|} = \chi_{40}/\chi_{20}^2, \quad \mathrm{Ex}_{\perp} = \chi_{04}/\chi_{02}^2,$$

$$\beta_{22} = \chi_{22}/(\chi_{20}\chi_{02}). \qquad (4)$$

Here, R_p is the projective range of ions, $\triangle R_p$, $\triangle Y$ are the longitudinal and lateral stragglings, Sk is the skewness, β_{12} is the characteristic of a correlation between the projective range and lateral straggling, $\mathrm{Ex}_{\|}$, $\mathrm{Ex}_{\perp}$ are the longitudinal and lateral excesses, β_{22} is the same as β_{12} for the stragglings. Further, we assume that any distribution parameter has the same order, as the higher cumulant is relevant to it in Eq.(4). It should be noted also that $\chi_{20} > 0$ and $\chi_{02} > 0$ because they are the dispersions of a distribution [9]; and the excesses are connected with kurtosises calculated by TRIM [4, 11] as $\mathrm{Ex} = K - 3$.

Now a general distribution function can be found by the inverse Fourier transformation of Eq.(3) for ions implanted from a point source at the origin of coordinates. After some simple transformations, we obtain

$$\Pi_p(\vec{r},E) = \frac{1}{\pi^3\sqrt{\chi_{20}}\chi_{02}}\int_0^{\infty}\int_0^{\infty}\int_0^{\infty}\exp\Big[-\frac{s^2+t^2+q^2}{2} +$$

$$+\frac{1}{4!}(s^4\mathrm{Ex}_{\|} + (t^2+q^2)^2\mathrm{Ex}_{\perp} + 6s^2(t^2+q^2)\beta_{22})\ldots\Big]\times$$

$$\times\cos\left[\frac{yt}{\sqrt{\chi_{02}}}\right]\cos\left[\frac{zq}{\sqrt{\chi_{02}}}\right]\cos\left[\frac{\chi_{10}-x}{\sqrt{\chi_{20}}}s -\right.$$

$$-\frac{s}{3!}\left(s^2\mathrm{Sk}+3(t^2+q^2)\beta_{12}\right)+\ldots\Bigg]dsdtdq, \tag{5}$$

and, after the transition to spherical coordinates in the $\vec{r}$-space and to polar coordinates in the inverse space and some evaluations,

$$\Pi_p(r,\theta,E)=\frac{1}{2\pi^2\sqrt{\chi_{20}}\chi_{02}}\int\limits_0^\infty\int\limits_0^\infty u\times$$

$$\times\exp\Bigg[-\frac{s^2+u^2}{2}+\frac{1}{4!}(s^4\mathrm{Ex}_{\|}+u^4\mathrm{Ex}_{\perp}+$$

$$+6s^2u^2\beta_{22})-\ldots\Bigg]\cos\left[\frac{\chi_{10}-r\cos\theta}{\sqrt{\chi_{20}}}s-\frac{s}{3!}(s^2\mathrm{Sk}+\right.$$

$$\left.+3u^2\beta_{12})+\ldots\right]J_0\left(\frac{r\sin\theta}{\sqrt{\chi_{02}}}u\right)dsdu, \tag{6}$$

where $J_0(x)$ is the Bessel function of the first kind. After the integration of Eq.(5) over all z and some manipulations, we obtain the distribution function in the case of a linear source placed on the z-axis:

$$\Pi_l(x,y,E)=\frac{1}{\pi^2\sqrt{\chi_{20}\chi_{02}}}\int\limits_0^\infty\int\limits_0^\infty\times$$

$$\times\exp\Bigg[-\frac{s^2+t^2}{2}+\frac{1}{4!}(s^4\mathrm{Ex}_{\|}+t^4\mathrm{Ex}_{\perp}+$$

$$+6s^2t^2\beta_{22})-\ldots\Bigg]\cos\left[\frac{yt}{\sqrt{\chi_{02}}}\right]\cos\left[\frac{\chi_{10}-x}{\sqrt{\chi_{20}}}s-\right.$$

$$\left.-\frac{s}{3!}\left(s^2\mathrm{Sk}+3t^2\beta_{12}\right)+\ldots\right]dsdt. \tag{7}$$

Analogously, after the integration of Eq.(7) over all y, we obtain the distribution function for ions supplied by an unconfined flat source placed on the Oyz surface,

$$\Pi_s(x,E)=\frac{1}{\pi\sqrt{\chi_{20}}}\int\limits_0^\infty\exp\left[-\frac{s^2}{2}+\frac{1}{4!}s^4\mathrm{Ex}_{\|}-\ldots\right]\times$$

$$\times\cos\left[\frac{\chi_{10}-x}{\sqrt{\chi_{20}}}s-\frac{1}{3!}s^3\mathrm{Sk}+\ldots\right]ds, \tag{8}$$

which coincides with the total range distribution obtained in [1]. In order to find a distribution in the case of a flat source restricted by a closed contour C, it is necessary to substitute $y\Rightarrow y-y'$ and $z\Rightarrow z-z'$ into Eq.(5) and then to integrate over y' and z' in the area inside the contour.

It is necessary to note that Eqs. (5)—(8) define distributions in a formal way. In order to evaluate the obtained expressions, one should find the sums of series for the real and imagine parts in Eq.(3) or under an exponent and a cosine in Eqs.(3)—(8) [1, 5]. The polynomial approximations of the series are possible only up to the square terms in u, v, w [5], and they give the Gauss distribution

$$\Pi_{222}(x,y,z,E)=\frac{1}{\pi\sqrt{\chi_{20}}}\,e^{-\frac{(\chi_{10}-x)^2}{2\chi_{20}}-\frac{y^2+z^2}{2\chi_{02}}} \tag{9}$$

for the quadratic approximation, or the Dirac δ-distribution $\Pi_{111}(\vec{r},E)=\delta(x-\chi_{10})\delta(y)\ \delta(z)$ for the linear one.

Although Eqs.(5)—(8) are formal, they together with Eqs. (3), (4) display the influence of higher-order cumulants on a distribution function. For example, two positive χ_{30} and χ_{12} always decrease the coefficient in the square brackets of the imaginary part in Eq.(3). It is equivalent to a decrease of χ_{10}. Therefore, a distribution with these parameters will have a maximum shifted to the left in respect to the Gaussian. If $\chi_{30}<0$ and $\chi_{12}<0$, the maximum will be shifted to the right. All positive $\chi_{40},\chi_{04},\chi_{22}$ increase the real part of Eq. (3), which is equivalent to a decrease of χ_{20},χ_{02}. This means that a distribution with these parameters will be narrower than the Gaussian. Analogously, if $\chi_{40},\chi_{04},\chi_{22}<0$, then a distribution will be wider than the Gaussian. For the different cumulant signs, their influence on a distribution is not obvious. The influence of the omitted fifth-order cumulants can be analyzed analogously. It is opposite to the influence of the third-order ones and decreases it. Further, the influence of the sixth-order cumulants is opposite to the influence of the fourth ones and also decreases it, and so on. Below, we show that the influence of higher moments on lower ones can change them significantly.

2. LSS Equations for Cumulants

The relations between moments and cumulants are well known [5, 9]. Therefore, it is possible to find the LSS equations for cumulants χ_{ij} using those for moments T_{lmn} [3] or parameters p_k^n [6]. The obtained equations for all cumulants of some order N will be interlinked. To

avoid this, let us introduce the so-called ersatzcumulants η_{ij} [1,10] as the linear combinations of cumulants:

$$\eta_{11} = \chi_{10}, \quad \eta_{02} = \chi_{20} + 2\chi_{02}, \quad \eta_{22} = \chi_{20} - \chi_{02},$$

$$\eta_{13} = \chi_{30} + 2\chi_{12}, \quad \eta_{33} = \chi_{30} - 3\chi_{12},$$

$$\eta_{04} = \chi_{40} + \frac{8}{3}\chi_{04} + 4\chi_{22},$$

$$\eta_{24} = \chi_{40} - \frac{4}{3}\chi_{04} + \chi_{22}, \quad \eta_{44} = \chi_{40} + \chi_{04} - 6\chi_{22},$$

where the second index j shows the order of ersatzcumulants and corresponding cumulants and moments, the first index $i \leq j$ has the same parity as j and defines the order of a Legendre polynomial on the left-hand sides of the corresponding equations. The ersatzcumulants are just some substitutions and, therefore, they do not have a simple physical interpretation in opposite to the usual parameters in Eq. (4).

Then the LSS equations for each ersatzcumulant η_{ij} can be written down and three first and simplest of them are

$$\hat{\mathcal{L}}\eta_{11}(\varepsilon) = 1,$$

$$\hat{\mathcal{L}}\eta_{02}(\varepsilon) = \frac{1}{\gamma}\int_0^{\varepsilon} \sigma(\varepsilon,\tau)\frac{\partial}{\partial\tau}\left[\eta_{11}\left(2\eta_{11}(\varepsilon)P_1(\nu) - \eta_{11}\right)\right] d\tau,$$

$$\hat{\mathcal{L}}\eta_{22}(\varepsilon) = \frac{1}{\gamma}\int_0^{\varepsilon} \sigma(\varepsilon,\tau)\frac{\partial}{\partial\tau}[\eta_{11}(2\eta_{11}(\varepsilon)P_1(\nu) -$$

$$-\eta_{11}P_2(\nu))]d\tau, \qquad (10)$$

with the left-hand sides defined as

$$\hat{\mathcal{L}}\eta_{ij}(\varepsilon) \equiv -\frac{1}{\gamma}\int_0^{\varepsilon} \sigma(\varepsilon,\tau)\frac{\partial}{\partial\tau}\left[\eta_{ij}P_i(\nu)\right] d\tau + S_e(\varepsilon)\eta'_{ij}(\varepsilon), \qquad (11)$$

where ε is the dimensionless ion energy [3, 6], $t \equiv \gamma\tau$ is the dimensionless lost energy, $\gamma = 4\mu/(1+\mu)^2$, $\mu = A_1/A_2$, A is the atomic weight, indices 1 and 2 denote ion and target atoms, respectively, $\eta_{ij} \equiv \eta_{ij}(\varepsilon - \gamma\tau)$, $P_i(x)$, $i = 0, 1, 2, \ldots$ are Legendre polynomials,

$$\nu \equiv \nu(\varepsilon, t) = \frac{\mu+1}{2\mu}(1 - t/\varepsilon)^{1/2} + \frac{\mu-1}{2\mu}(1 - t/\varepsilon)^{-1/2}$$

is the cosine of a scattering angle, $S_e(\varepsilon)$ is the electronic stopping, and

$$\sigma(\varepsilon,\tau) = \int_{\tau}^{\varepsilon} d\sigma(\varepsilon,\tau')$$

is the so-called summarized cross section of nuclear collisions of an ion with initial energy ε, where it loses the energy from some $t \equiv \gamma\tau$ up to the maximum value $t_{\max} \equiv \gamma\tau_{\max} = \gamma\varepsilon$ [1].

We do not reproduce here the rest of equations as they are very cumbersome, but we underline that they always have the form

$$\hat{\mathcal{L}}\eta_{ij}(\varepsilon) = \frac{1}{\gamma}\int_0^{\varepsilon} \sigma(\varepsilon,\tau)\frac{\partial}{\partial\tau}F_{ij}\left(\nu, \eta_{kl}, \eta_{mn}(\varepsilon)\right) d\tau, \qquad (12)$$

where F_{ij} are some polynomial functions of the scattering angle and lower-order ersatzcumulants with $l, n < j$, which are similar to the functions on the right-hand sides of Eq.(10).

From Eqs. (10), (12), we can see that all cumulants starting from the second-order one appear only due to the influence of high-order moments of nuclear scattering. At low energies $\varepsilon \ll 1$, the integrals on the right-hand sides are large only when integrands are large. This may happen only for a large scattering angle. Since it is true for light ions, their distributions significantly deviate from a Gaussian at low energies. At high energies $\varepsilon \gg 1$, the integrals are large only when their upper limits are large. Therefore, the distributions significantly deviate from a Gaussian both for light and heavy ions at high energies.

Equations (10)—(12) differ from the known LSS equations [3, 6] at the following points: 1) all right-hand sides are expressed explicitly through the nuclear scattering; 2) the differential cross section of the nuclear scattering $d\sigma(\varepsilon, t)$ is absent on both sides of equations, which is the advantage as it is essentially nonintegrable at the point $t = 0$; 3) terms that are formed only by $\eta_{ij}(\varepsilon)$ and increase very fast with the ion energy are also absent on the both sides of the equations; 4) the equations for the η_{0j}, where $j = 2, 4, 6, \ldots$, become the integral equations for functions η'_{0j}.

The first gives an advantage for the analysis of the experimental data on ion distributions, because the influences of the nuclear and electronic interactions on all the parameters are outlined explicitly [1]. From the physical point of view, it is the most important feature of the cumulant algorithm, because it gives a possibility to use the higher moments of the ion spatial distribution for a more precise definition of the ion-atom interaction. Last three differences allow developing a more stable and faster numerical method of solving Eqs. (10)—(12) than that known at the moment [1].

3. Results and Discussions

In this paper, we present the results of numerical calculations. The parameters of the spatial ion distribution for the implantation of Ni^+ into Fe which were calculated according to Eqs. (10)—(12) by the numerical algorithm which we call PSAL (Projected Semiinvariant Algorithm) [1] and by package TRIM [11] are shown in Table 1. The energy is measured in keV, the projected range R_p, the stragglings ΔR_p and ΔY, the lateral range $Y^{\rm MC}$ and $\sqrt{|\chi_{11}^{\rm MC}|}$ are measured in nm, and the rest of parameters are dimensionless.

For calculations, we have used a potential function and a screening radius according to Biersack—Ziegler and an electronic stopping according to the database SCOEFDATA [4, 11]. Electronic straggling for the chosen ion and target atom can be omitted [3, 4]. The sample sizes for the TRIM calculations were equal to $n = 50000$ ions. It is worth noting that the time for calculations of the presented data is about 10 CPU-hours for the TRIM and about 20 CPU-seconds for the PSAL on a processor with the frequency equal to 800 MHz.

Parameters with index MC (Monte Carlo simulations by TRIM) have been calculated in several stages. First, the coordinates of a final point for every ion x_i, y_i, z_i, $i = 1, \ldots, n$, have been found by TRIM. Then the spatial moments have been calculated, and finally the cumulants have been found using the well-known formulas [5, 9]. It appeared that all calculated MC-parameters are not equal to zero. However, some of them must vanish according to the axial symmetry of the distribution. There are several reasons for this contradiction: 1) the finite sample size; 2) the numerical rounding of the results in TRIM (Digits=4); 3) the imperfection of a random number generator. To

Parameters of spatial distribution of Ni^+ ions implanted into Fe. For the each ion energy, the first row is the results of PSAL; the second and the third rows are the results obtained by TRIM

E	R_p	ΔR_p		ΔY	Sk	β_{12}	$\mathrm{Ex}_{\parallel}$		β_{22}		$\mathrm{Ex}_{\perp}$
	$R_p^{\rm MC}$	$\Delta R_p^{\rm MC}$		$\Delta Y^{\rm MC}$	$\mathrm{Sk}^{\rm MC}$	$\beta_{12}^{\rm MC}$	$\mathrm{Ex}_{\parallel}^{\rm MC}$		$\beta_{22}^{\rm MC}$		$\mathrm{Ex}_{\perp}^{\rm MC}$
	$\lvert Y^{\rm MC}\rvert$		$\sqrt{\lvert\chi_{11}^{\rm MC}\rvert}$		$\lvert\mathrm{Sk}_{\perp}^{\rm MC}\rvert$	$\lvert\beta_{21}^{\rm MC}\rvert$		$\lvert\beta_{31}^{\rm MC}\rvert$		$\lvert\beta_{13}^{\rm MC}\rvert$	
1	1.184	0.710		0.584	0.7292	0.3160	0.6010		0.2627		1.071
	1.281	0.646		0.630	0.5347	0.1822	0.0513		0.0896		0.3634
	0.0		0.02		0.02	0.01		0.02		0.03	
10	4.839	2.690		2.213	0.5958	0.2899	0.2779		0.1720		0.8644
	5.015	2.539		2.258	0.5522	0.2250	0.1646		0.0932		0.5046
	0.0		0.07		0.01	0.01		0.01		0.01	
20	7.932	4.248		3.495	0.5356	0.2786	0.1486		0.1320		0.7882
	8.212	4.073		3.547	0.4914	0.2381	0.0072		0.0804		0.5065
	0.01		0.34		0.01	0.00		0.02		0.05	
50	16.34	8.169		6.756	0.4247	0.2510	−0.0435		0.0641		0.6455
	16.65	7.930		6.846	0.4023	0.2158	−0.1305		0.0183		0.5257
	0.01		0.42		0.02	0.00		0.01		0.01	
100	29.88	13.88		11.63	0.3023	0.2155	−0.1987		−0.0003		0.5010
	30.15	13.56		11.84	0.2982	0.1987	−0.2337		−0.0129		0.4081
	0.03		0.79		0.01	0.01		0.01		0.06	
200	57.11	24.04		20.67	0.1336	0.1617	−0.3248		−0.0704		0.3262
	57.32	23.69		20.88	0.1338	0.1452	−0.3436		−0.0826		0.2838
	0.02		0.87		0.01	0.00		0.00		0.01	
500	142.1	49.82		45.14	−0.1647	0.0625	−0.3050		−0.1402		0.0883
	141.4	49.07		45.41	−0.1570	0.0486	−0.3493		−0.1334		0.0308
	0.07		1.81		0.00	0.00		0.00		0.02	
10^3	285.0	82.66		79.76	−0.4579	−0.323	0.0181		−0.1478		-0.0512
	282.7	81.94		79.69	−0.4310	−0.0326	−0.0650		−0.1335		−0.0688
	0.23		5.92		0.01	0.01		0.01		0.07	
10^4	1794	206.3		267.2	−1.671	−0.3439	5.198		0.3381		0.0555
	1793	208.0		263.1	−1.653	−0.3304	5.022		0.3029		0.0555
	1.41		4.54		0.00	0.01		0.09		0.27	
10^5	7048	251.1		388.8	−3.163	−0.5764	26.97		2.220		1.012
	7071	253.6		384.9	−3.240	−0.5490	29.10		2.044		0.9133
	0.91		26.91		0.00	0.04		0.89		0.37	
10^6	73810	469.9		903.9	−36.10	−2.301	2777		77.50		17.45
	74647	516.6		869.4	−37.70	−1.798	3061		29.21		17.28
	5.44		88.16		0.20	0.26		29.19		12.44	

illustrate the influence of these factors on the absolute errors of TRIM calculations, we also display the values of characteristic parameters in the third row for each energy. So, $|Y^{\rm MC}|$ determines the error of $R_p^{\rm MC}$, $\sqrt{|\chi_{11}^{\rm MC}|}$ determines the error of $\Delta R_p^{\rm MC}$ and $\Delta Y^{\rm MC}$, and so on.

The numerical errors of the PSAL calculations can be controlled with different algorithm settings as described in [1]. They are less than about 3% for all given data for energies more than 10 keV, but they can attain up to 10% for the third and fourth order parameters for lower energies.

From Table 1, one can see that the results of calculations by the PSAL-algorithm and by the MC-modelling qualitatively coincide. The quantitative coincidence is observed when the ion energy increases and the order of parameters decreases. This is because the influence of the ion backscattering that is included in the TRIM calculations is not taken into account in the LSS theory. But this effect is significant only at low ion energies. For energies higher than 20 keV, the number of backscattered ions is less than 0.5% and the first five parameters coincide within this accuracy. The remaining differences between the TRIM and PSAL results in the table, especially for higher orders, are explained by approximations used in both methods: the extrapolation errors for PSAL [1]; the piece-straight-line approximation of an ion trajectory in TRIM [4]. It must be noted that, for light ions implanted into a heavy target when $\mu \ll 1$, the discrepancies between TRIM and PSAL calculations are about 25%. The reason for this is that we did not take into account the electronic straggling in the presented PSAL version.

Our calculations for many different ion-target combinations and various interaction potentials, screening radii, and electronic stoppings showed the following features of the dependences of the distribution parameters on the ion energy: 1) they are all positive for low energies, when the nuclear scattering dominates; 2) only the first and second order parameters increase always with energy, but all the others decrease at low energies; 3) the third order parameters decrease and reach zero, and further they become negative for very high energies, when the electronic stopping dominates; 4) the fourth order parameters decrease at low energies, and then they become negative and reach a minimum. Further, they increase and become large positive for high energies; 5) the parameters of the total range distribution behave analogously [1]. Our study of the parameters up to the eighth order has shown that the number of zeros N_z on the energy axis for a cumulant and its order N are related as

$$N_z = N - 2 \quad \text{for} \quad N \geq 2. \tag{13}$$

We have also tested the validity of this relationship for parameters of a spatial distribution up to the fourth order by calculations within PSAL and TRIM. If this formula remains valid for the all higher parameters, they become more and more oscillating functions of energy with increase of their order. But since the distribution varies continuously with change in energy, the contribution of these moments must be accumulated into the second characteristic function in Eq.(4) in such a way that it must smoothen the dependence on energy.

This behaviour of parameters can influence their values that are fitted to experimental data for the implanted impurity distribution. For example, for a high energy of projectiles, their distribution created by a flat source is shifted to the right and is narrower concerning a Gauss distribution. Therefore, if these experimental data are approximated by a Gaussian, this leads to an overestimating of $R_p^{\rm exp}$ and an underestimating of $\Delta R_p^{\rm exp}$. For intermediate energies where $Sk \approx 0$, $\mathrm{Ex}_{\|} < 0$ always, and this leads to an overestimating of values of $\Delta R_p^{\rm exp}$. For low energies, the fitting errors are opposite to ones for high energies. If one uses the Pearson distribution, the analogous errors for skewness will appear because of the influence of higher-order cumulants. Moreover, when a fitted projective range is overestimated (underestimated), skewness must be overestimated (underestimated) too, because it shifts a maximum of the fitted distribution to left (right) and cancels right (left) shifts of the maximum caused by such a range. Deviations of both parameters from the true values should be proportional according to properties of the Pearson distribution.

The examples of such a cross influence of fitted parameters are presented in Fig. 1,*a,b*. There are experimental data (circles) for the distribution parameters of ions Mo implanted into Si obtained in [13] by fitting their spatial distribution with the Pearson-IV distribution; the results of PSAL-calculations (lines) and TRIM-simulations (crosses) are obtained with the above settings. It is obvious that the results of our calculations and TRIM-simulations practically coincide and the behaviour of the experimental data qualitatively testifies to the described cross correlated errors.

The analogous relation between the longitudinal straggling and the excess is also valid and can be seen in Fig. 1,*c,d*. However, in [13], the excess did not fit to experimental distributions, and instead the approxima-

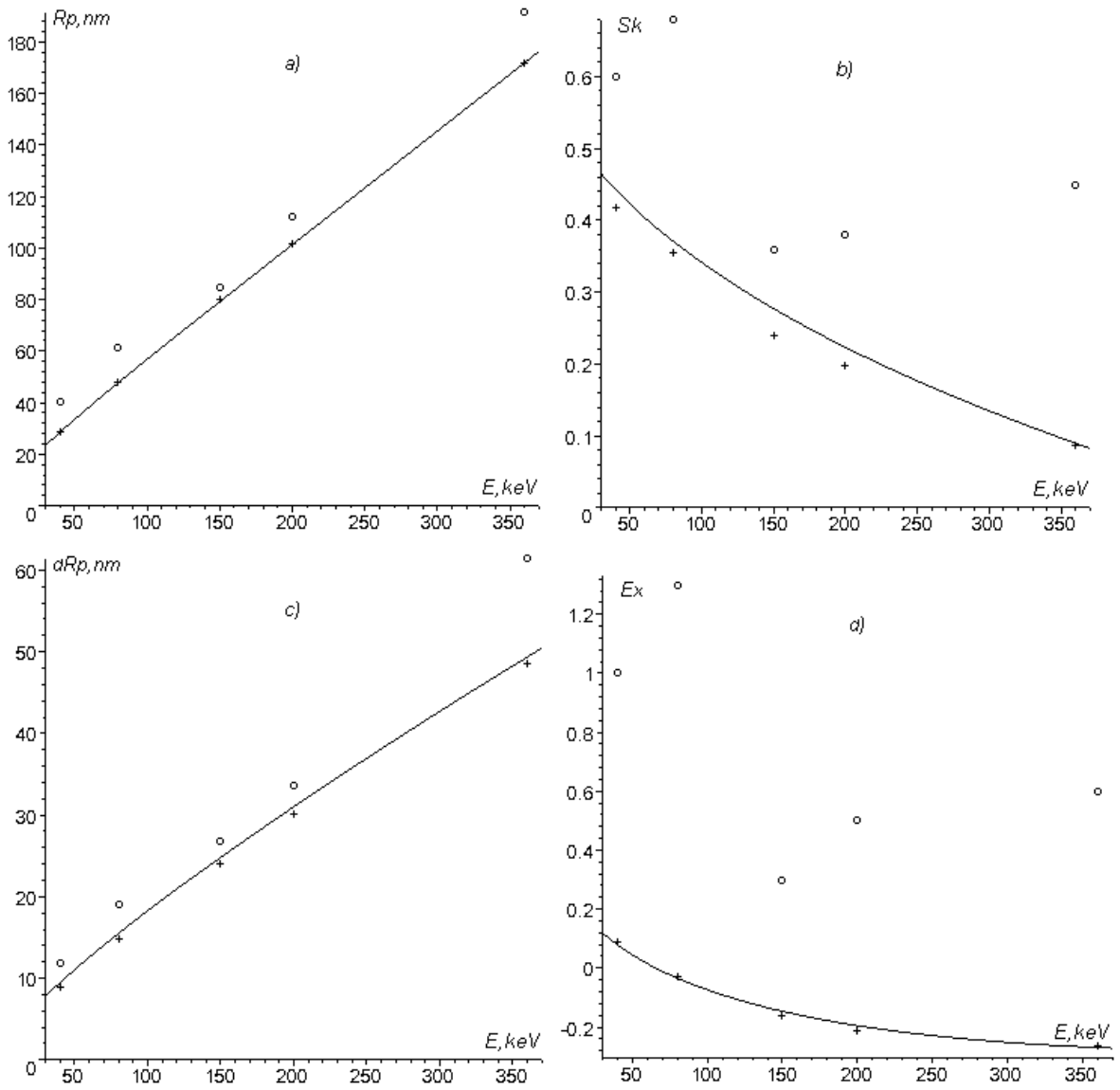

Fig. 1. Energy dependences of the distribution parameters for Mo implanted into Si. Experimental data — ∘, PSAL-calculation — lines, TRIM-simulations — ×; *a* — the projective range, *b* — skewness, *c* — longitudinal straggling, *d* — longitudinal excess

tion Ex = −0.2 + 2.4Sk was used. Therefore, we cannot use the experimental data to obtain numerical estimations of the correlated errors. However, our calculations of the Pearson-IV distribution with the experimental data and the Pearson distribution which corresponds to the PSAL parameters in Fig. 1 show a reasonable coincidence within two stragglings near the maximum.

Thus, the parameters of the impurity distribution obtained by fitting the theoretical curve to experimental data have cross correlated errors. The higher-order parameters always have systematic errors depending on the projectile energy.

In Fig. 2, the dependences of the dimensionless first derivatives of ersatzcumulants $\eta'_{kn}(\varepsilon)$ for the combination $Ni^+ \rightarrow Fe$ are shown. These derivatives are basic functions in the PSAL algorithm and all others quantities are related to them. It is obvious from Fig. 1 that they are not monotonic functions of energy. We have found that the observed change in the monotonic

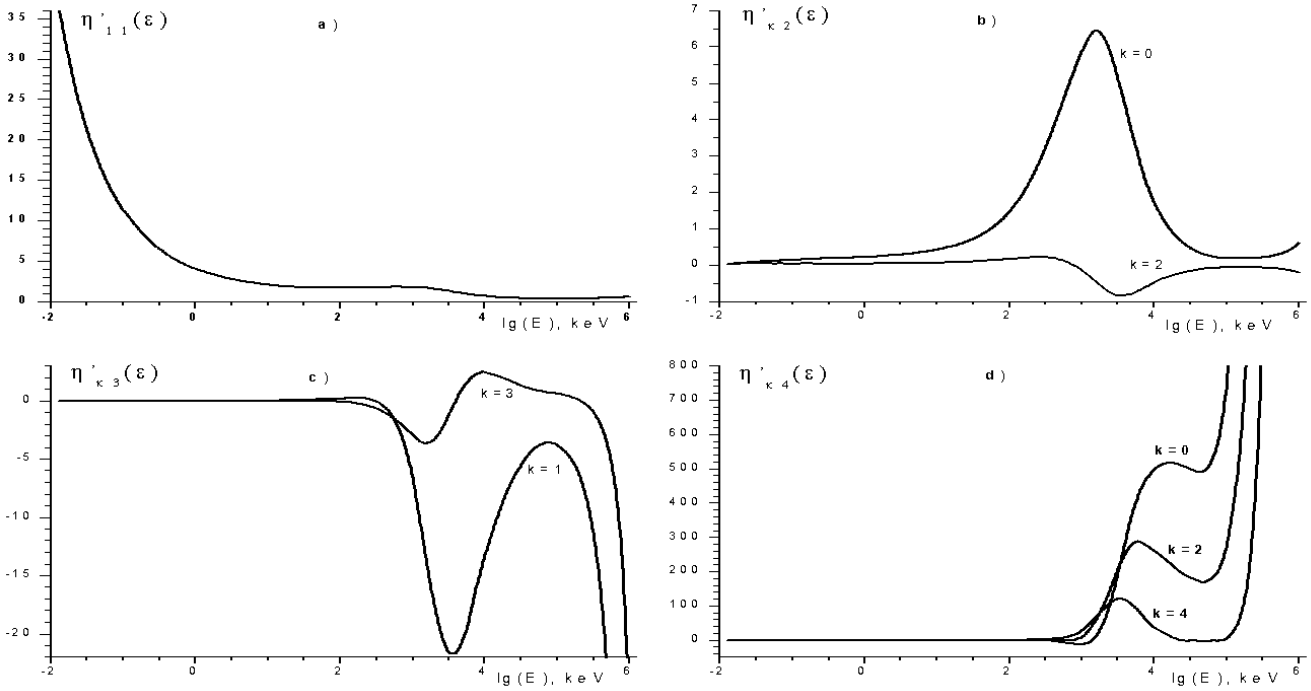

Fig. 2. Energy dependence of the dimensionless first derivative of ersatzcumulants $\eta'_{kn}(\varepsilon)$ for Ni implanted into Fe (E in keV): a — $n = 1$; b — $n = 2$; c — $n = 3$; d — $n = 4$. The index k is shown near each curve

behavior happens near the energy $\varepsilon^\star$, where the effective nuclear scattering approximately equals the electronic stopping. As was shown in [12], the derivative of the projective range can be written down with reasonable accuracy as

$$\eta'_{11}(\varepsilon) \sim \frac{1}{S_t(\varepsilon)} + O(\gamma),$$

where $S_t(\varepsilon) = S_e(\varepsilon) + S_n^{\rm ef}(\varepsilon)$ and $S_n^{\rm ef}(\varepsilon) = S_n(\varepsilon)(\mu+1)/\mu$ is the so-called effective nuclear scattering. This allows estimating the above-mentioned energy approximately as $\varepsilon^* \approx 2 \div 8$ for all ion-target combinations. Fig. 2,*a* shows that the effective total stopping of Ni ions in a random Fe target decreases when the ion energy increases from about 60 up to 320 keV. By using the analogy with total cumulants [1], we can assume that solutions of the integral equations (10)—(12) also can be approximated qualitatively with solutions of the differential equations:

$$\eta'_{kn}(\varepsilon) \sim \gamma^{n-1} \frac{\Psi_{kn}(\mu,\varepsilon)}{S_t(\varepsilon)^{n+1}} + O(\gamma^n), \quad n \geq 2,$$

where $\Psi_{kn}(\mu,\varepsilon)$ are combinations of nuclear scattering moments and electronic stopping which are similar to ones obtained in [1]. According to this formula, increasing the monotonically changing amplitudes $\eta'_{kn}(\varepsilon)$ in Fig. 2,*b*—*d* is stipulated by the decrease of $S_t(\varepsilon)$, and the sign change of $\eta'_{kn}(\varepsilon)$ is stipulated by the sign change of $\Psi_{kn}(\mu,\varepsilon)$. Therefore, these changes, namely their amplitudes and the zeros and extrema of derivative functions are sensitive to fine details of the electronic stopping and nuclear scattering. This opens the possibility to use the spatial distribution moments higher than the first one for the analysis of ion-atom interaction. However, the discussion of the results [13] shows that a sensible and accurate method for the determination of higher moments of a distribution has not else been developed.

Conclusions

Thus, the cumulant method applied in this paper to the spatial distributions of implanted ions allowed us to create an accurate and fast algorithm for the calculation of distribution parameters. The energy dependences of the higher order parameters are oscillating functions, and these parameters must be included into an

empirical distribution in a way that will smoothen the energy function. The influence of higher moments can stipulate significant errors for all parameters if they are obtained by fitting the empirical distribution to the experimental one. The method offers the possibility of a more precise determination of ion-atom interaction details through the analysis of higher moments.

This research has been supported partially by INTAS grant No 2136.

1. *Makarets' M.V., Storchaka S.M.* // Ukr. Fiz. Zh. — 2001.— **46**, N4. — P.486 — 492.
2. *Kunert T., Schmidt R.* // Phys. Rev. Lett. — 2001. — **86**, N23. — P.5258 — 5261.
3. *Lindhard J., Scharf M., Schiott H.E.* // Mat. Fys. Med. Dan. Vid. Selsc. — 1963. —**33**, N14. — P.1 — 53.
4. *The Stopping* Power and Range of Ions in Matter/ Ed. J.E. Ziegler. — New York: Pergamon Press, 1985. — Vol.1.
5. *Malakhov A.N.* Cumulant Analysis of Random Non-Gauss Processes and Its Transformations. — Moscow: Sovetskoe Radio, 1978 (in Russian).
6. *Burenkov A.F., Komarov F.F. Kumahov, M.A., Temkin M.M.* Spatial Distribution of Energy Deposited on Collision Cascade in Solid. — Moscow: Energoatomizdat, 1985 (in Russian).
7. *Bowyer M.D.J., Asworth D.G., Oven R.* //J. Phys. D **29** (1996) 1274.
8. *Bowyer M.D.J., Asworth D.G., Oven R.*//Ibid. 1286.
9. *Korn G.A., Korn T.M.* Mathematical Handbook. — M.: Nauka, 1974 (in Russian).
10. *Ilyina V.V., Makarets N.V.* // Proc. XII IMRPSS/ Ed. G.G. Bondarenko. — Moscow: SRI PMT, 2002.
11. *Web page:* http:/www.srim.org.
12. *Makarets N.V.* // Microelectronica. — 1990. — **19**, N3. — P.293 — 296.
13. *Liang J.H.*// Jpn. J. Appl. Phys. — 1999. — **38**, Pt.1, N1A. — P.286 — 290.

Received 30.07.03

КУМУЛЯНТНИЙ АНАЛІЗ РОЗПОДІЛУ ІМПЛАНТОВАНИХ ІОНІВ

В.В. Ільїна, М.В. Макарець

Р е з ю м е

Метод аналізу рівнянь Ліндхарда—Шарффа—Шіотта, раніше запропонований авторами для розподілу повних пробігів імплантованих іонів, використано для пошуку параметрів їхнього просторового розподілу. Одержано інтегральні рівняння для перших восьми кумулянтів і знайдено їх чисельні розв'язки для однокомпонентних мішеней в діапазоні енергій від 100 еВ до 1 ГеВ. Встановлено загальні закономірності в залежностях параметрів розподілу від енергії іонів, показано, що підгонка розподілів до експериментальних даних може зумовлювати значні скорельовані похибки знайдених параметрів. Метод дозволяє врахувати всі моменти розподілу для знаходження атом-атомної взаємодії.